DALTON
FULL PAPER

Geometries and segregation properties of platinum–palladium nanoalloy clusters †

Claire Massen, Thomas V. Mortimer-Jones and Roy L. Johnston *

School of Chemical Sciences, University of Birmingham, Edgbaston, Birmingham, UK B15 2TT. E-mail: roy@tc.bham.ac.uk

Received 12th August 2002, Accepted 26th September 2002
First published as an Advance Article on the web 29th October 2002

A detailed study is made of Pt, Pd and Pt–Pd bimetallic clusters, $(PtPd)_M$, with up to 56 atoms, modelled by the many-body Gupta potential. A Genetic Algorithm is used to find the lowest energy structures for each nuclearity and composition. A variety of structure types (icosahedral, decahedral, fcc close-packed and disordered) are observed for Pt clusters. The Pd clusters have similar geometries to those of Pt, though more icosahedral clusters and fewer disordered structures are found than for Pt. Global minima are generally more difficult to find for the bimetallic Pt–Pd clusters, due to the presence of homotops (structures with identical geometries but with different arrangements of the Pt and Pd atoms) as well as geometrical isomers. The structures found for the bimetallic clusters are different to those of either of the pure element clusters, with more decahedral structures and fewer icosahedra. Segregation is observed in the Pt–Pd clusters, with most having Pt-rich cores and Pd-rich surfaces. This is explained in terms of the lower surface energy of Pd and the higher cohesive energy of Pt. Doping of Pt atoms into Pd clusters (and *vice versa*) is found to lead to significant changes in cluster geometry. The effect of varying the Pt–Pd parameters of the Gupta potential on the geometrical structures and atomic segregation in Pt–Pd clusters is investigated and the parameters obtained by averaging the Pt–Pt and Pd–Pd parameters are found to give best agreement with experiment. Our results are generally in good agreement with previous experimental and theoretical studies of Pt, Pd and Pt–Pd clusters and related alloy systems.

1 Introduction

1.1 Nanoalloy clusters

Clusters are aggregates of between a few and many millions of atoms or molecules. They may consist of identical atoms, or molecules, or two or more different species and can be studied in a number of media, such as molecular beams, the vapour phase, in colloidal suspensions and isolated in inert matrices or on surfaces.[1] Interest in clusters arises, in part, because they constitute a new type of material which may have properties which are distinct from those of discrete molecules or bulk matter: for example, metals (such as palladium) which are non-magnetic in the solid state can give rise to non-zero magnetic moments in discrete clusters.[1–3] Another reason for the interest in clusters is the size-dependent evolution of cluster properties.[1,4,5]

The range of properties of metallic systems can be greatly extended by taking mixtures of elements to generate intermetallic compounds and alloys.[6] In many cases, there is an enhancement in specific properties upon alloying, due to synergistic effects, and the rich diversity of compositions, structures and properties of metallic alloys has led to widespread applications in electronics, engineering and catalysis. The desire to fabricate materials with well defined, controllable properties and structures, on the nanometre scale, coupled with the flexibility afforded by intermetallic materials, has generated interest in bimetallic alloy clusters – or 'nanoalloys'.[7,8,9]

One of the major reasons for interest in nanoalloy particles is the fact that their chemical and physical properties may be tuned by varying the composition and atomic ordering, as well as the size of the clusters. Their surface structures, compositions and segregation properties[10,11] are of interest as they are important in determining chemical reactivity, and especially catalytic activity.[12,13] Nanoalloy clusters are also of interest as they may display structures and properties which are distinct from those of the pure elemental clusters. There are also examples of pairs of elements (such as iron and silver) which are immiscible in the bulk phase but which readily mix in finite clusters.[14]

A number of theoretical studies, mainly using empirical many-body potentials, have been performed on intermetallic clusters (see, for example, refs. 8, 9, 15–19). Calculations based on semi-empirical molecular orbital methods and Density Functional Theory (DFT) have also been applied to the study of small bimetallic clusters (see, for example, refs. 20–22).

1.2 Platinum and palladium catalysts

In this paper, we describe a theoretical study of the structures, stabilities and atomic ordering in platinum (Pt) and palladium (Pd) clusters, and in mixed Pt–Pd nanoalloy clusters. Platinum and palladium are of interest because they are widely used as catalysts (often as finely divided metal particles, in elemental or alloy form) in a number of important reactions – many involving hydrogenation. They are used, for example, in catalytic converters in automobiles, for the reduction of exhaust gases. A review of the effects of co-metals in catalysis by Pd-based alloys has been presented by Coq and Figueras.[23]

An important catalytic application of Pt and Pd is in the reduction (by hydrogenation) of aromatic hydrocarbons in fuel. This process, however, suffers from the problem of catalyst poisoning by H_2S, formed from sulfur-containing impurities in the fuel. It has been claimed that Pt–Pd alloy particles are more catalytically active for aromatic hydrocarbon hydrogenation and more resistant to sulfur-poisoning than either of the pure

† Electronic supplementary information (ESI) available: all of the global minima for Pt_{10}–Pt_{55} and Pd_{10}–Pd_{55} clusters. See http://www.rsc.org/suppdata/dt/b2/b207847c/

metals (*i.e.* there is said to be synergism),[24] though Renouprez, Rousset and co-workers have challenged these conclusions, stating that the most important interaction is likely to be that between the metallic particle and the alumina or silica support.[25,26]

Before describing our results, we present a brief overview of some of the previous work (both experimental and theoretical) on Pt, Pd and Pt–Pd clusters.

1.3 Previous studies of Pt, Pd and Pt–Pd clusters

1.3.1 Pt clusters. Sachdev *et al.* calculated the structures of Pt clusters, using the many-body Embedded Atom Method (EAM) – starting with icosahedral and cuboctahedral structures and compared these with structures found by Monte Carlo Simulated Annealing (MCSA).[27] They found that relaxing the icosahedral and cuboctahedral clusters caused them to become irregular and defective, but also more compact and spherical. The MCSA search found less symmetrical isomers with lower energies than the icosahedral and cuboctahedral clusters even for the 'magic numbers' of 13 and 55 atoms, where the icosahedron and cuboctahedron have closed geometric shells and so are expected to be particularly stable. They also discovered many other structures with energies similar (*i.e.* within 0.1 eV atom^{-1}) to those of the global minimum (GM) which are also more disordered than the icosahedron. Doye and Wales used the Sutton–Chen (SC) many-body potential and Monte Carlo minimization to predict the structures of Pt clusters with up to 80 atoms. They found the icosahedron to be the GM for Pt_{13}, but for other sizes they found GM with close-packed (face-centred cubic) fcc (the structure of bulk Pt), decahedra and disordered (or 'amorphous') structures.[28]

Small Pt clusters (with up to 8 atoms) have been studied in detail by several groups. Using another EAM potential, Yang *et al.* found that planar structures were preferred for $Pt_{4–6}$ (a W-shape for Pt_5 and a triangular shape made up of four small triangles for Pt_6), with 3-dimensional bipyramids as metastable isomers for Pt_5 and Pt_6.[29] Kua and Goddard predicted that Pt_6 has a structure composed of edge-sharing tetrahedra, while Pt_7 and Pt_8 are planar.[30] Except for the disagreement concerning Pt_6, both of these investigations suggest that small platinum clusters are planar.

Although Pt_{13} has been widely studied, there is no concensus as to the lowest energy structure for this cluster. Sachdev *et al.* found a disordered GM from EAM studies,[27] as did Yang *et al.*[29] and Lin *et al.* (from DFT calculations).[31] An icosahedral GM was, however, found by García-Rodeja *et al.*[32] and by Uppenbrink and Wales,[33] using alternative EAM potentials, though Uppenbrink and Wales also found many distorted structures that were close in energy to the GM. Corrected Effective Medium (CEM) theory was used to perform molecular dynamics (MD) simulations of Pt clusters by Yang and DePristo.[34] Two similar potentials gave two different GM structures, the icosahedron and another, more open and distorted, structure. Watari and Ohnishi compared the cuboctahedron and the icosahedron at the DFT level, using the generalised gradient approximation to the exchange correlation potential and spin-orbit coupling including Jahn–Teller effects.[35] They predicted the cuboctahedron to be more stable than the icosahedron, in agreement with the studies of Yang *et al.*,[29] though Yang *et al.* found many disordered structures with lower energies than the cuboctahedron.

At present, it is often not possible to determine the structures of clusters unambiguously in the gas phase or in a molecular beam.[1] Structural determination techniques therefore involve supporting the clusters either on a surface or in an inert matrix, both of which may affect the structure of the cluster. Most electron microscopy studies of supported Pt particles have shown them to adopt fcc packing (as in bulk Pt), with the morphology of the particle depending on the preparation conditions.[36] Contrata *et al.* bombarded silica-supported platinum clusters of less than 4 nm diameter with electrons from a scanning tunnelling electron microscope.[37] After bombardment, the clusters were disordered and remained amorphous for up to 24 hours. This proves that amorphous Pt clusters can exist under certain experimental conditions, though they may not necessarily be GM.

1.3.2 Pd clusters. Using an EAM potential, Sachdev *et al.* found that magic number Pd clusters with 13 or 55 atoms had icosahedral GM, but that for other nuclearities the GM were not icosahedral, though icosahedral-type structures often lie close in energy to the GM.[27] Reddy *et al.* carried out geometry optimization calculations on high-symmetry icosahedral and octahedral structures and found the icosahedron to be the most stable.[2] CEM calculations by Stave and DePristo for Pd_N clusters ($N \leq 23$) found GM with structures based on icosahedral packing for most nuclearities,[38] with the results being most similar to those obtained for Ni, rather than Pt. Efremenko has noted that DFT calculations have provided conflicting results for the structure of Pd_{13}, though his own Tight Binding calculations indicate that the GM for Pd_{13} is icosahedral, with the cuboctahedral isomer lying very close in energy.[39]

High-resolution electron microscopy studies by Penisson and Renou have shown that small Pd particles are icosahedral,[40] while José-Yacamán *et al.* found fcc cuboctahedral, twinned, decahedral and amorphous structures for particles with diameters of 1–5 nm.[41] For larger particles, fcc structures are generally found.[36] Efremenko has noted that there is a tendency for pentagonal symmetry and twin formation for highly-dispersed Pd deposits on different supports, in thin films, in Pd-containing alloys and even in the gas phase.[39]

1.3.3 Pt–Pd clusters. Bulk Pt–Pd alloys are continuous solid solutions – *i.e.* structures in which the atoms are randomly mixed, with no segregation, for all compositions.[42] This is consistent with the relatively low enthalpy of formation of $Pt_{0.5}Pd_{0.5}$ (-4 kJ mol^{-1}), for example, when compared with -59 kJ mol^{-1} for ordered (bcc) NiAl.[42] The pure elements and the bulk alloy phases exhibit fcc packing of atoms and cubic symmetry ($L1_2$).[6]

Renouprez, Rousset and colleagues have performed extensive experimental studies of the structures, compositions and catalytic activity of Pt–Pd particles generated by the laser vaporization of bulk alloys of various compositions.[25,26] From, transmission electron microscopy, the Pt–Pd particles (which typically have diameters in the range 1–5 nm) were found mainly to have cuboctahedral structures, with fcc packing, as in the bulk alloy phases. EDX measurements showed that the overall compositions of the particles are very similar to those of the alloys used as the laser vaporization target. EXAFS measurements showed that the Pt–Pd particles are alloyed, but that there are more Pt–Pt interactions than expected for a Pt–Pd solid solution. This indicates that some segregation has occurred relative to the bulk alloys. Low energy ion scattering experiments have shown that the surfaces of these Pt–Pd particles are enriched in Pd, relative to a homogeneous distribution of Pt and Pd atoms, with the relative enhancement being largest for low average Pd concentrations and for larger particles. It was also found that Pd atoms are etched preferentially upon ion bombardment, which is consistent with there being proportionally more Pd atoms on the surface of the clusters to start with.

To our knowledge, there have been no previous calculations on Pt–Pd nanoalloy clusters. We will make comparisons with previous theoretical studies of other nanoalloy systems (*e.g.* Cu–Au, Ni–Al and Cu–Pd) below.

1.4 Homotops

On going from pure metal clusters to bimetallic nanoalloys, there is an increase in complexity, due to the presence of two different types of atoms, which leads to the possibility of isomers based on the permutation of unlike atoms, as well as the usual geometrical isomers (with different skeletal structures). Jellinek has introduced the term 'homotops' to describe A_aB_b alloy cluster isomers, with a fixed number of atoms ($N = a + b$) and composition (a/b ratio), which have the same geometrical arrangement of atoms, but differ in the way in which the A- and B-type atoms are arranged.[9,19] As the number of homotops rises combinatorially with cluster size, global optimization (in terms of both geometrical isomers and homotops) is an extremely difficult task. For a 20-atom $A_{10}B_{10}$ cluster, for example, there are 184 756 homotops, though many may be symmetry-equivalent. The maximum total number of homotops of any composition for a given structural isomer is 2^N, which for a 20-atom cluster is approximately 10^6.[43] Depending on the symmetry of the cluster, however, many of these homotops may be symmetry-equivalent and it is possible that a significant number of permutations will give rise to unstable arrangements – *i.e.* not corresponding to local minima on the potential energy hypersurface.

1.5 Genetic algorithms

Whether one is using empirical potentials or *ab initio* theory to describe the bonding in clusters, one of the principal objectives is to find, for a given cluster size, the arrangement of atoms (or ions or molecules) corresponding to the lowest potential energy – *i.e.* the GM on the potential energy hypersurface. However, as the number of minima rises quasi-exponentially with increasing cluster size, finding the GM becomes increasingly difficult.[44] In the discussion presented below, although it can never be guaranteed that the GM for a particular cluster size and composition has been found, we will label the lowest energy structure as the GM, for convenience.

The Genetic Algorithm (GA)[45,46] is a search technique based on the principles of natural evolution. It employs operators that are analogues of the evolutionary processes of genetic crossover, mutation and natural selection to explore multi-dimensional parameter spaces. A GA can be applied to any problem where the variables to be optimized ('genes') can be encoded to form a string ('chromosome'), each string representing a trial solution of the problem. The GA operators exchange information between the strings to evolve new solutions. The GA approach operates in an essentially parallel manner – different regions of parameter space are investigated simultaneously, with information concerning different regions of parameter space being passed between the individual strings by the crossover procedure. In this way, genetic information is disseminated throughout the population.

Here, we report the application of a Genetic Algorithm to determine the structures and atomic distributions in pure elemental Pt and Pd clusters with up to 55 atoms and in Pt–Pd nanoalloy particles with up to 56 atoms, with all interactions modelled by the Gupta many-body potential.[47] A review of previous applications of GAs for cluster optimization has been presented elsewhere.[48]

2 Methodology

2.1 The Gupta potential

Since, for large clusters (of hundreds or thousands of atoms) *ab initio* calculations are still, at present, unfeasible (at least if large areas of configuration space are to be searched), there has been much interest in developing empirical atomistic potentials for the simulation of such species. Empirical potentials, such as the Gupta potential,[47] are derived by fitting experimental data to values calculated using a potential of an assumed functional form. The Gupta potential, which is based on the second moment approximation to Tight Binding theory, is written in terms of repulsive (V^r) pair and attractive many-body (V^m) terms, which are obtained by summing over all (N) atoms:

$$V_{\mathrm{clus}} = \sum_{i}^{N} \left\{ V^{\mathrm{r}}(i) - V^{\mathrm{m}}(i) \right\} \quad (1)$$

where

$$V^{\mathrm{r}}(i) = \sum_{j}^{N}{}' A(a,b) \exp\left(-p(a,b)\left(\frac{r_{ij}}{r_0(a,b)} - 1 \right) \right) \quad (2)$$

and

$$V^{\mathrm{m}}(i) = \left[\sum_{j}^{N}{}' \zeta^2(a,\ b) \exp\left(-2q(a,b)\left(\frac{r_{ij}}{r_0(a,b)} - 1 \right) \right) \right]^{\frac{1}{2}} \quad (3)$$

In eqns. (2) and (3), r_{ij} is the distance between atoms i and j in the cluster and A, r_0, ζ, p and q are fitted to experimental values of the cohesive energy, lattice parameters and independent elastic constants for the reference crystal structure at 0 K. The primes indicate summation over all atoms j, except $j = i$.

2.1.1 Gupta parameters. For Pt_xPd_y alloy clusters, the parameters take different values for each of the different types (Pt–Pt, Pd–Pd and Pt–Pd) of interaction. In the above equations, a and b are the atom labels for atoms i and j respectively. The homonuclear (Pt–Pt and Pd–Pd) parameters were derived by fitting to the pure metals[47] and are taken to be unchanged in the alloys. These parameters are listed in Table 1.

In the Gupta potential, the parameters p and q (or more strictly the ratios p/r_0 and q/r_0) can be thought of as measures of the ranges of the repulsive and attractive interactions respectively: the larger their value the shorter the range (*i.e.* the more rapidly the pair or many-body energy contributions die off with increasing interatomic separation). Thus p/r_0 is slightly larger for Pd (3.95) than for Pt (3.82). This, coupled with the larger value of the A parameter for Pt, means that the pair term is more repulsive for Pt than Pd for a given number and arrangement of atoms [since the metallic radii, and hence the interatomic distances of Pd (r = 1.38 Å) and Pt (r = 1.39 Å) are so similar[49]]. Turning to the attractive many-body part of the potential, Pd now has a longer range parameter (smaller q/r_0) but a smaller hopping integral (ζ) than Pt. The cohesive energy of bulk Pd (3.936 eV) is significantly smaller than that of Pt (5.853 eV),[47] presumably because the larger ζ value for Pt–Pt interactions overcomes both the higher value of q/r_0 and the increased 2-body repulsion energy. As has previously been shown for related potentials,[28] the ranges of pair and many-body energy terms are important in determining the relative stabilities of different cluster geometries.

2.1.2 Choosing Pt–Pd parameters. Heteronuclear Pt–Pd interaction parameters have not previously been derived for the

Table 1 Gupta potential parameters for calculations on Pt–Pd clusters. The Pt–Pt and Pd–Pd parameters are those derived by Cleri and Rosato.[47] (See text for discussion of Pt–Pd parameter sets **I**, **II** and **III**)

	Pt–Pt	Pd–Pd	Pt–Pd(**I**)	Pt–Pd(**II**)	Pt–Pd(**III**)
A/eV	0.2975	0.1746	0.23	0.35	0.23
ζ/eV	2.695	1.718	2.2	2.2	3.0
p	10.612	10.867	10.74	10.74	10.74
q	4.004	3.742	3.87	3.87	3.87
r_0/Å	2.7747	2.7485	2.76	2.76	2.76

Gupta potential. As the stoichiometric 1:1 Pt–Pd alloy is a solid solution ($Pt_{0.5}Pd_{0.5}$), rather than an ordered intermetallic, it was decided to generate the Pt–Pd parameters by taking averages of the Pt–Pt and Pd–Pd parameters instead of fitting the cohesive energies and elastic properties of the alloy. It was found that, by rounding to two decimal places (for A, p, q and r_0) or one decimal place (for ζ), the arithmetic and geometric means were the same, so these rounded averages were used as our initial Pt–Pd parameters. They are listed in Table 1 as Pt–Pd(**I**). These Pt–Pd parameters have been used for most of the calculations on Pt–Pd clusters reported below.

The adoption of averaged parameters for the heteronuclear interactions was driven by the knowledge that the bulk Pt–Pd alloys are solid solutions – with $Pt_{0.5}Pd_{0.5}$, for example, having a very small exothermic enthalpy of formation (-4 kJ mol^{-1})[42] – and also by the fact that in other alloy systems the parameters are sometimes close to average values and generally lie between the limits of the homonuclear interaction parameters.[47] Of course, the use of averaged parameters is a significant approximation and, in future studies, it would be interesting to modify these parameters by including data on bulk Pt–Pd alloys in the fitting procedure. In the meantime, we have chosen to investigate the effect of varying the Pt–Pd parameters on the structures of a limited set of Pt–Pd clusters, with the Pt:Pd ratio fixed at 1:1. The modified parameter sets were obtained from the averaged set **I**: by increasing the 2-body energy scaling parameter (A), such that A(Pt–Pd) > A(Pt–Pt) > A(Pd–Pd) [denoted Pt–Pd(**II**) in Table 1]; and by increasing the many-body energy scaling parameter (ζ), such that ζ(Pt–Pd) > ζ(Pt–Pt) > ζ(Pd–Pd) [denoted Pt–Pd(**III**) in Table 1]. In both cases, all other parameters are left unchanged. These extreme changes (*i.e.* making the heteronuclear parameter lie outside the homonuclear values) are very simplistic, but should give an idea of the relative importance of the pair and many-body interactions in the Gupta potential.

2.2 Cluster energetics

From the total cluster potential energy V_{clus}, the average binding energy for an N-atom cluster is defined as the positive quantity:

$$E_b = \frac{-V_{clus}}{N} \tag{4}$$

and the second difference in binding energy may be calculated as:

$$\Delta_2 E_b(N) = 2E_b(N) - E_b(N+1) - E_b(N-1) \tag{5}$$

where $\Delta_2 E_b(N)$ represents the relative stability of an N-atom cluster with respect to its neighbours (*i.e.* clusters with $N - 1$ and $N + 1$ atoms).

2.3 The genetic algorithm for cluster geometry optimization

As our cluster geometry optimization GA has been described in detail previously,[48,50] only a brief description is presented here.

For a given cluster nuclearity (N), a number of clusters, N_{pop}, are generated at random and then energy-minimized (using the limited memory quasi-Newton L-BFGS routine[51]) to form the initial population (the 'zeroth generation'), where each member of the population now corresponds to a local minimum on the potential energy hypersurface. This simplification of the surface has been shown to greatly facilitate the search for the global minimum by reducing the space that the GA has to search.[48] The same principle underpins the Basin Hopping Monte Carlo method developed by Doye and Wales[52] and the 'Monte Carlo plus energy minimization' approach of Li and Scheraga.[53]

After all of the clusters have been energy-minimized, each cluster is assigned a fitness value, based on its total potential energy (V_{clus}), such that low energy clusters (more negative V_{clus}) have high fitness and high energy clusters (less negative V_{clus}) have low fitness. In this work we have studied exponential (exp) and hyperbolic tangent (tan$h$) fitness functions, where the fitness (F_i) of the ith member of the population (with $V_{clus} = V_i$) is given by:

$$F_i = \exp(-3\rho_i) \tag{6}$$

and

$$F_i = \frac{1}{2}\left[1 - \tanh\left(2\rho_i - 1\right)\right] \tag{7}$$

respectively. The dimensionless quantity:

$$\rho_i = \frac{V_i - V_{min}}{V_{max} - V_{min}} \tag{8}$$

and V_{max} and V_{min} are the V_{clus} values of the highest and lowest energy clusters in the current population.

The selection of parents for mating is accomplished using a variant of the roulette wheel method, whereby a cluster is picked at random and is accepted for mating if its fitness value (F_i) is greater than a randomly generated number between 0 and 1. If the candidate cluster is rejected for mating, then another is picked and the process is repeated. In this way, low energy clusters (with high fitness values) are more likely to be selected for mating and, therefore, to pass on their structural characteristics. Once a pair of parents have been selected for mating, they are subjected to the crossover operation.

Crossover is carried out using a modified version of the slice and splice crossover operator of Deaven and Ho,[54] in which random rotations (about two perpendicular axes) are performed on both parent clusters and then both clusters are cut horizontally – parallel to the xy plane – and complementary fragments are spliced together.

In this study, three ways of slicing the clusters have been considered:

- **Random**—a single slice plane is generated with a random z coordinate.
- **Weighted**—a single slice plane is generated, with its z coordinate weighted according to the relative fitnesses of the two parent clusters.
- **Double**—two slice planes are generated with random z coordinates.

Complementary slices are then combined to generate offspring, with only one offspring being considered in our implementation. For heteroatomic clusters, such as nanoalloy clusters, the crossover procedure has been modified in order to preserve the correct number of atoms of each type in the cluster.[55,56] Unless selected for mutation, each offspring cluster is subsequently locally minimized.

While the mating/crossover operation leads to a mixing of genetic material in the offspring, no new genetic material is introduced. In an attempt to maintain population diversity, a mutation operator is introduced. In our GA, mutation is performed on the set of N_{mat} offspring, with each offspring cluster having the same probability (P_{mut}) of being mutated.

Here, four mutation operations have been studied:

- **(Cluster) Replacement**—the selected cluster is eliminated and replaced by a new, randomly generated cluster.
- **(Atom) Displacment**—approximately $\frac{1}{3}$ of the atoms in the selected cluster are moved to new, randomly generated positions.
- **(Cluster) Twisting**—the top half of the selected cluster is rotated by a random angle about the z axis, relative to the bottom half.
- **(Atom) Permutation**—swaps the atom types (in a pairwise fashion) of approximately $\frac{1}{3}$ of the atoms in the selected cluster,

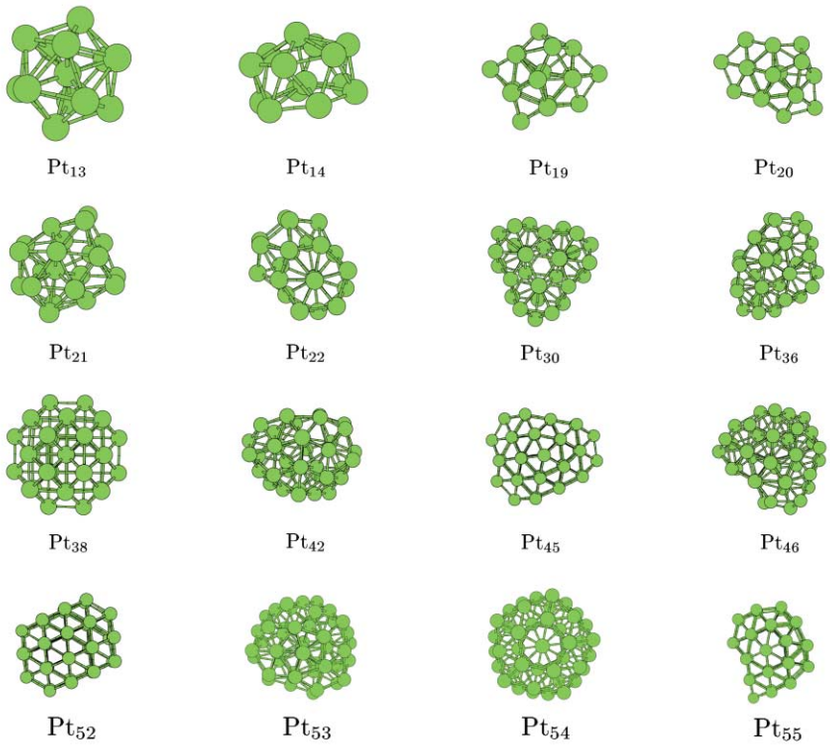

Fig. 1 GM for selected Pt clusters with 13–55 atoms. (All of the GM in the range 10–55 atoms can be found as ESI †.)

without changing the cluster geometry. This type of mutation is only used for hetero-atomic clusters, such as nanoalloys, because for single element clusters it does not lead to any change.

After mutation, the new ('mutant') clusters are locally minimized.

The next stage of the GA involves selecting the N_{pop} lowest energy clusters to form the next generation. The set of N_{pop} 'old' clusters (from the previous generation) and N_{mat} 'new' clusters (offspring and mutants) are ranked in order of potential energy. The top N_{pop} clusters (*i.e.* those with lowest energy) are then selected to constitute the next generation. This is an example of 'elitist' selection.

The whole process of mating, mutation and selection is repeated for a specified number (N_{gen}) of generations.

The values of the GA parameters used in all calculations reported here were: N_{pop} = 30; N_{mat} = 24; P_{mut} = 0.1. The maximum number of generations allowed (N_{gen}) varied from 100 to 400, increasing with cluster nuclearity (N). For each value of N and composition (for Pt–Pd clusters, where appropriate), 10 GA runs were performed, using different, randomly generated initial populations.

3 Results and discussion

3.1 Optimization of GA operations

Before calculating the GM for mono- and bi-metallic clusters with up to 56 atoms, a number of tests were performed to compare the efficiency of the various alternative fitness functions and crossover and mutation operators described above. Calculations were carried out for selected Pd, Pt and Pt–Pd clusters with 10–40 atoms. In each case, the efficiency was gauged by running the GA ten times, using different, randomly generated initial populations, and observing how often the lowest energy cluster isomer (the assumed GM) was found within 100 generations.

Overall, there was not found to be a very large difference in GA efficiency upon changing the fitness function, with the tanh function giving slightly better results for the Pt and Pt–Pd test cases, and the exp function performing better for Pd clusters. For small Pd and Pt clusters, the type of crossover operator adopted did not make much difference, though random single slice crossover was slightly better for larger Pd clusters, such as Pd_{35}, and double slice crossover was better for larger Pt clusters, such as Pt_{40}. In the case of the Pt–Pd clusters, random single slice crossover was again found to be slightly more reliable. Considering the alternative mutation operators, for the Pd and Pt clusters small differences were again observed, with atom displacement mutation giving slightly better results for Pd and cluster replacement mutation being a little more efficient for Pt. For the Pt–Pd clusters, atom displacement and atom permutation mutation were found to be competitive.

Although small differences were found in the performance of the GA upon changing the fitness function and crossover/mutation operators, it was decided to use, for each type of cluster, the best combination identified in these initial tests. For the Pt–Pd nanoalloy clusters, seperate GA runs were carried out using the atom displacement and permutation operators.

3.2 Elemental clusters

3.2.1 Pt clusters. The lowest energy structures (the assumed GM) found for selected clusters in the range Pt_{13}–Pt_{55}, are shown in Fig. 1. (All of the GM in the range Pt_{10}–Pt_{55} can be found as ESI †.) A variety of structures can be seen. Many of the clusters (N = 10–13, 22–32, 36, 42, 44–49, 53 and 54) have structures based on icosahedral or distorted icosahedral packing. Closed geometric shell Mackay icosahedra are possible for N = 13 and 55. For the Gupta Pt potential, the icosahedron is found to be the GM for Pt_{13}; however, the GM for Pt_{55} is not icosahedral, rather it has a low-symmetry disordered structure. The icosahedral isomer of Pt_{55} was calculated to be metastable, with a binding energy (E_b) which is 2.5 meV atom^{-1} lower than that of the GM.

In our calculations, clusters with $15 < N < 20$ have structures based on a truncated decahedral (bicapped pentagonal prismatic) core. The square faces between the pentagons are generally capped first because these are more open, and capping these faces means that the capping atoms have a coordination

number of 4, rather than 3 (when a triangular face is capped). At larger sizes, close-packed fcc structures (*i.e.* the same packing as in bulk Pt) are observed: N = 33–35, 38–40 and 50–52. The GM for Pt_{38} has the familiar truncated octahedral geometry, previously found for 38-atom clusters of Cu and Au, using the Gupta potential.[55] Pt_{50} is a twinned truncated octahedron. A number of disordered structures, such as Pt_{48}, Pt_{49} and Pt_{55}, have also been identified.

Pt_{14} has a hexagonal antiprismatic structure, with two atoms displaced from the centres of the hexagonal planes, in the same direction along the six-fold axis (so an alternative description is a capped centred hexagonal antiprism). This structure has previously been identified as the GM for Au_{14} using both the Gupta potential[55] and the Murrell–Mottram (MM) many-body potential.[57] Pt_{21} has a 3-layer double hexagonal antiprismatic structure, again with all central atoms displaced in the same direction along the six-fold axis. It is evident, however, that adding a capping atom to the open hexagonal face (to generate a possible structure for Pt_{15} and Pt_{22}) does not lead to a stable structure.

Our results are consistent with those of Sachdev *et al.*,[27] in that the structures are generally not based on icosahedra, although we found an icosahedron for N = 13 whereas they found an irregular structure. Our structure for N = 55 is similar to that of Sachdev *et al.*,[27] neither being icosahedral. Whereas most of the Sachdev structures are disordered, as mentioned above, we have found a number of regular structures in addition to disordered structures. The structures that we have found for smaller clusters are: Pt_5 – trigonal bipyramid; Pt_6 – octahedron; Pt_7 – pentagonal bipyramid; and Pt_8 – bicapped octahedron. These are inconsistent with the results of Yang *et al.*[29] and Kua and Goddard[30] (which predicted mainly planar structures for the smaller clusters), presumably because explicit electronic effects (such as Jahn–Teller distortions and π-bonding) are missing from the empirical Gupta potential.

In their calculations using the SC potential, Doye and Wales also found the icosahedron to be the lowest energy structure for Pt_{13}.[28] As in this study, for certain other nuclearities they found some close-packed and decahedral structures rather than icosahedra. Again in agreement with our study, they found hexagonal antiprismatic structures for Pt_{14} and Pt_{21}, rather than the icosahedral-based structures which are commonly obtained for other metals (*e.g.* Ag, Rh, Ni and Cu). Most of our structures are very similar, if not identical, to those found by Doye and Wales.

We have recently found the lowest energy structures of gold clusters using a Gupta potential and the same GA as in this study.[55] For Au clusters, again the icosahedron was found to be the GM for Au_{13} and a disordered structure was found for Au_{55} (though a different structure to that found here for Pt_{55}). Hexagonal antiprism structures were also obtained (for N = 14 and 21), along with a (reduced) number of close-packed structures (*e.g.* the truncated octahedron for Au_{38}) and the same 3-fold symmetric triply-fused icosahedral structure for N = 30. The observed similarity between the GM found for Au and Pt clusters, using the Gupta potential, can be understood by noting the similarity in the pair and many-body range exponents (p and q) for these two elements, which are listed in Table 2.[47] Interestingly, Doye and Wales have shown that, for the many-body SC potential, Pt and Au clusters have identical structures, as the SC pair and many-body range exponents are the same for these two elements.[28]

By fitting the calculated cluster binding energies (E_b) to the following cubic equation in $N^{-1/3}$:

$$E_{\text{fit}} = a + bN^{-1/3} + cN^{-2/3} + dN^{-1} \qquad (9)$$

it is possible to obtain an estimate (as $N \longrightarrow \infty$) of the binding energy of an infinite cluster (*i.e.* a), which should equal the cohesive energy (E_{coh}) of the bulk solid. The value of a obtained for Pt is 6.0412 eV, which is only 3% higher than the value of E_{coh} for fcc Pt (5.853 eV) used by Cleri and Rosato in fitting the Pt potential.[47] This accuracy is good, especially since only clusters with up to 55 atoms have been used in the extrapolation.

Table 2 Comparison of Gupta potential parameters for fcc metals of groups 10 and 11 [47]

	Ni	Pd	Pt	Cu	Ag	Au
A/eV	0.0376	0.1746	0.2975	0.0855	0.1028	0.2061
ζ/eV	1.070	1.718	2.695	1.224	1.178	1.790
p	16.999	10.867	10.612	10.960	10.928	10.229
q	1.189	3.742	4.004	2.278	3.139	4.036
r_0/Å	2.4911	2.7485	2.7747	2.5562	2.8885	2.8843

A plot of the difference between the fit to eqn. (9) and the calculated binding energies ($E_{\text{fit}} - E_b$) is shown in Fig. 2(a). This shows that small clusters with nuclearities of 6 and 7, and clusters with nuclearities of 13 (icosahedron), 30 (triply-fused icosahedron) and 38 (truncated octahedron) are particularly stable, showing up as large negative values on this graph. Clusters with N = 11, 12, 14, 21 and 31 are all relatively unstable, which may be because they have non-spherical structures and not many bulk-like (encapsulated) atoms. The second differences in the binding energies ($\Delta_2 E_b$) are plotted against N in Fig. 2(b). Large positive peaks in $\Delta_2 E_b$ (as for N = 13, 30 and 38) show clusters which are stable with respect to their neighbours, correlating well with the large negative troughs in $E_{\text{fit}} - E_b$. High negative values of $\Delta_2 E_b$ (indicating relatively unstable structures) are found for N = 12, 14, 21 and 31, correlating with positive peaks in Fig. 2(a).

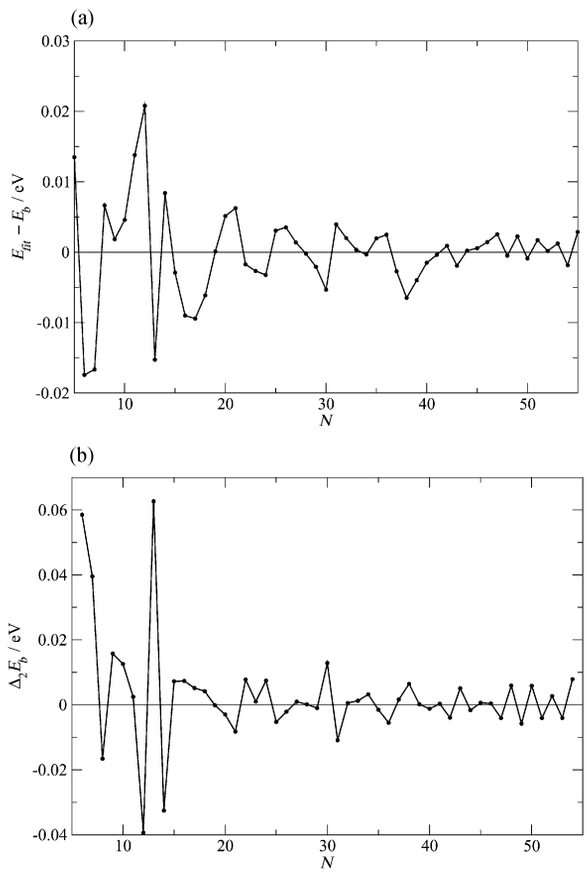

Fig. 2 (a) Plot of $E_{\text{fit}} - E_b$ as a function of cluster nuclearity, N, for Pt clusters. (b) Plot of $\Delta_2 E_b$ as a function of N for Pt clusters.

3.2.2 Pd clusters. The GM found for selected clusters in the range Pd_{13}–Pd_{55} are shown in Fig. 3. (All of the GM in the

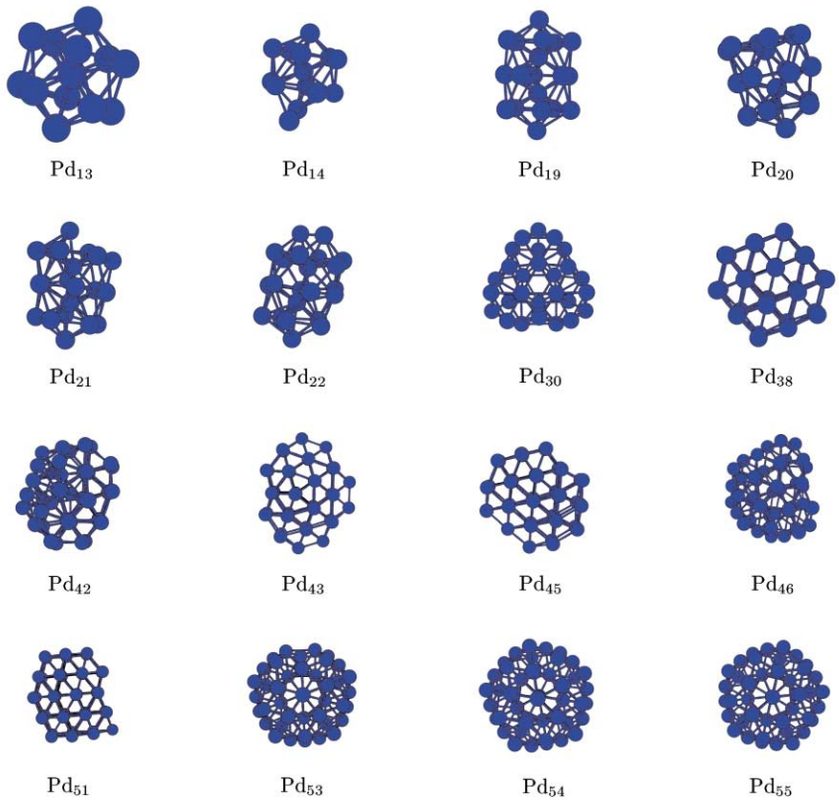

Fig. 3 GM for selected Pd clusters with 10–55 atoms. (All of the GM in the range 10–55 atoms can be found as ESI †)

range Pd_{10}–Pd_{55} can be found as ESI †.) The GM structures are generally similar to those found for the Pt clusters. The main differences are that for Pd clusters there are more structures based on icosahedral packing than for Pt and there are fewer disordered structures (examples are found for Pd clusters with around 42 atoms). This increased tendency for Pd to form icosahedral-based structures has previously been predicted on the basis of calculations using the MM many-body potential.[58] The GM for Pd_{19}, for example, is a double icosahedron (DI) and similar structures are found in this size regime. The DI structure has previously been found to be the GM for 19-atom clusters of Cu, Ni and Al, using Gupta potentials.[55,56,59] Pd_{14} has a capped icosahedral structure, in contrast to the hexagonal antiprismatic structure found for Pt_{14}. Also in contrast to Pt, the GM for Pd_{55} is an ordered closed shell Mackay icosahedron, rather than a disordered structure. Pd_{54} has the same, uncentred icosahedral structure as Pt_{54}, but Pd_{53} has an icosahedral structure with one vertex and one central atom missing, as compared with Pt_{53}, which has two outer-shell atoms missing from the icosahedron and is distorted. As for Pt, structures with fcc packing are observed for 38–41-atom Pd clusters and for certain higher nuclearities (*e.g.* Pd_{45} and Pd_{51}).

Sachdev *et al.* also identified icosahedra as the GM for Pd_{13} and Pd_{55}.[27] However, these were the only icosahedral clusters that they found. They also noted a marked difference between the structures of Pd and Pt clusters, whereas our structures are somewhat more similar. As they do not include structures for all cluster nuclearities in their paper, a full comparison is not possible – but their structures for Pd_{20} and Pd_{30} are similar (but not identical) to the ones shown in Fig. 3. Interestingly, Sachdev *et al.* do not mention the 19- and 23-atom DI structures, indicating perhaps that they were not found – which would be consistent with our results for Pt, though not for Pd.

Although the GM for Pd_{19} is the DI, the lowest energy isomers of Pd_{20} and Pd_{21} are not the simple waist-capped and bi-capped DI structures previously found, for example, for Cu clusters.[55] The Pd_{20} GM has a structure with rings of 5, 6 and 6 metal atoms, with one exposed axial atom, one internal atom and one slightly recessed axial atom. The Pd_{21} GM is derived from Pd_{20} by the addition of an off-axis capping atom on the top hexagonal face. The Pd_{22} GM can be generated by capping the hexagonal face of Pd_{20} with a Pd_2 fragment. The 20–22-atom Pd clusters can therefore be described as intermediates between DI-based strutures (as observed for Cu and certain other metals[55,56,59]) and the hexagonal antiprismatic structures of Pt_{21} and Au_{21}.[55] In a recent study of acetylene polymerization on small Pd_N clusters ($1 \leq N \leq 30$) supported on MgO, Abbet *et al.*[60] proposed a structure for the Pd_{20} cluster based on previous calculations on a model Morse potential.[50] The structure proposed is different from that predicted here for the GM of Pd_{20} – so perhaps this new structure could be used in future models of catalytic activity of Pd_{20}. Finally, it should be noted that our results are consistent with those of José-Yacamán *et al.*, whose high resolution electron microscopy studies revealed a variety of cluster types – fcc close-packed, icosahedral, decahedral and amorphous – for Pd nanoparticles of diameter 1–5 nm.[41]

Fitting the calculated binding energies of Pd_5–Pd_{55} to eqn. (9), gives a value for a of 4.1944 eV for Pd, which is only 6.5% higher than the value of E_{coh} for fcc Pd (3.936 eV) used by Cleri and Rosato in fitting the Pd potential.[47] Again, this represents good accuracy, considering that only clusters with up to 55 atoms have been used in the fitting. A plot of the difference between the fit to eqn. (9) and the calculated binding energies ($E_{fit} - E_b$) is shown in Fig. 4. Particularly stable clusters (large negative values) are evident at $N = 6$, 7, 13 and 38. Significant peaks are also observed for these nuclearities in a plot (not shown) of the second difference in the binding energies ($\Delta_2 E_b$) against N. These clusters have the same geometries as their Pt counterparts and their stability may likewise be attributed to their high symmetry and closed geometric shell nature. The plots in Figs. 2(a) and 4 are quite similar, though the oscillations about $E_{fit} - E_b = 0$ tend to be smaller for Pd than Pt. A notable exception is Pd_{13}, which is particularly stable – perhaps reflecting the greater tendency towards icosahedral structures for Pd clusters, as compared to Pt. Finally, Pd_{30} (which has the same

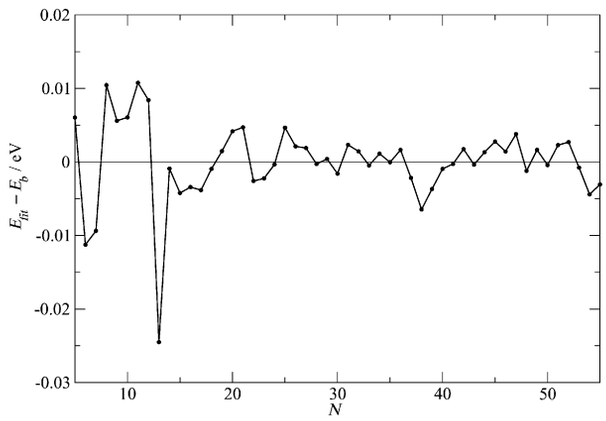

Fig. 4 Plot of $E_{fit} - E_b$ as a function of N for Pd clusters.

compact, triply-fused icosahedron structure as Pt_{30}) is again stable compared to its neighbours, though it does not stand out as much as its Pt analogue [see Fig. 2(a)].

3.2.3 Geometrically disordered *vs.* ordered structures. Calculations using the Gupta potential, by Michaelian, Garzón and co-workers[61,62] and by ourselves,[55] have led to the prediction that many gold clusters should have geometrically disordered (or 'amorphous') structures, and there is indeed experimental evidence for amorphous gold particles.[63] Michaelian, Garzón and co-workers subsequently carried out a detailed study of those factors which are responsible for stabilising amorphous over ordered structures in metal clusters.[64] It was concluded that the tendency for amorphization decreases with increasing cluster size (of course the bulk metals are crystalline) and that there is an increased tendency from left to right and from top to bottom of the periodic table, maximizing (for metallic elements) at gold.[64] A rough correlation was found to exist between the tendency to amorphization and the range of the pair and many-body components of the Gupta potential: thus larger values of the Gupta p and q parameters (shorter-ranged potentials) are associated with a greater tendency to adopt amorphous structures.[64] However, the competition between pair and many-body energies and their dependence on the relevant range exponent, makes it difficult to rationalise the tendency towards amorphization.

Soler *et al.* concluded that, next to Au, Pt and Pd (which have relatively high p and q parameters) should show the greatest tendency towards having amorphous clusters.[64] This is consistent with the non-icosahedral structures for Pt_{13} found in the calculations of Yang *et al.*[29] and Sachdev *et al.*[27] As noted above, there is also experimental evidence for amorphous Pt and Pd particles.[37,41] The Gupta potentials of Pt and Pd are compared with those of Au, Cu and Ni (Cu and Ni do not tend to form amorphous clusters[55,61]) in Table 2. More recently, Michaelian *et al.* have predicted that Pt_{38} should have a regular truncated octahedral (fcc) geometry, rather than being amorphous and have mapped out a band in p–q space which should give rise to amorphous structures.[65]

Our results, using the Gupta potential, for Pt and Pd clusters demonstrate that (in agreement with the prediction of Soler *et al.*[64]) there is indeed a tendency for Pt and Pd (to a lesser extent) to form disordered clusters. For Pt, the tendency is almost as great as for Au. As predicted by Michaelian *et al.*, however, Pt_{38} is found to adopt the ordered truncated octahedral geometry. It should be noted that in our study of Au clusters,[55] we found Au_{38} to be ordered (adopting the truncated octahedral geometry), in contrast to the findings of Michaelian, Garzón and co-workers.[61,66] This result is due to differences in the Gupta potentials used in these seperate studies, and the sensitivity of the Au_{38} to the Gupta parameters is confirmed by the results of Michaelian *et al.*, who have found Au to lie very close to the dividing line (in p–q space) between ordered and disordered structures for 38 atoms.[65]

Pd forms more icosahedral and other ordered clusters than either Au or Pt, but not as many as in the case of Ni and Cu.[55,61,67] Inspection of Table 2 reveals that the Gupta potential range parameters (p and q) for Pd lie between those of Au and Cu – with p(Pd) lying closer to p(Cu) and q(Pd) lying closer to q(Au)[47] – which would explain this intermediate behaviour. In fact, the p and q parameters for Pd are quite close to those of Ag, leading to the possibility that Pd and Ag clusters (as modelled by the Gupta potential) may have similar geometries.

3.3 Stoichiometric $(PtPd)_M$ nanoalloy clusters

3.3.1 Structures. The GM found, using the GA, for stoichiometric $(PtPd)_M$ clusters with M = 5–28 (*i.e.* N = 10–56 atoms) are shown in Fig. 5. Except for $(PtPd)_7$, which has a non-icosahedral, polytetrahedral structure, clusters with M = 5–12 (N = 10–24) have structures derived from the centred icosahedron. For larger clusters, however, there is a reduced tendency (when compared with Pt and Pd) to form icosahedral clusters. $(PtPd)_{21}$ and $(PtPd)_{22}$ do have structures based on icosahedral packing, but they are quite strongly distorted and may be regarded as disordered. In the size regime M = 13–18 (N = 26–36) a new structural motif is identified, with structures based on decahedral (pentagonal prismatic) cores. Such structures, which are similar to those found for 33–37-atom Pt and Pd clusters, have previously been identified as the GM for certain Au clusters,[55,57] as well as for clusters modelled by short-ranged Morse pair potentials.[50]

The $(PtPd)_M$ clusters generally have different structures to those of the corresponding pure Pt or Pd clusters. Exceptions include $(PtPd)_6$, which is an icosahedron with one vertex missing (as found for Pt_{12} and Pd_{12}), and $(PtPd)_{19}$ and $(PtPd)_{25}$, which have truncated octahedral and twinned truncated octahedral fcc-type structures, respectively (as found for the 38- and 50-atom Pd and Pt clusters). $(PtPd)_{20}$ also has a structure based on fcc packing, but it has a different geometry to that observed for Pt_{40} and Pd_{40}. The fcc structure of $(PtPd)_{26}$ is also different to that of fcc-Pt_{52} (Pd_{52} exhibits icosahedral packing). The GM for the largest cluster studied, $(PtPd)_{28}$, has a disordered structure, though there are regions of decahedral packing. The next lowest energy isomers of $(PtPd)_{28}$, however, are homotops of a structure consisting of a 2-shell 55-atom Mackay icosahedron, with a capping Pd atom. The low coordination of the capping atom destabilizes these isomers relative to the GM, which has no exposed atoms. The 54-atom $(PtPd)_{27}$ cluster has a distorted structure based on the 2-shell icosahedron with a surface atom missing.

In our previous study of Cu–Au clusters, we found that the geometries of stoichiometric $(CuAu)_M$ clusters resembled those of the pure Cu clusters quite closely, with a marked preference for icosahedral structures for all nuclearities, except $(CuAu)_{19}$, which adopts the ubiquitous truncated octahedral geometry.[55] This is in contrast to our findings for $(PtPd)_M$ clusters, which generally have structures which are distinct from those formed by either Pt or Pd. The reason for this difference presumably lies in the details of the balance between the A–A, B–B and A–B parameters in these $(AB)_M$ alloy systems. Finally, it is apparent from Fig. 5 that the lowest energy $(PtPd)_M$ isomers found for each nuclearity tend to have cores which are Pt-rich, with the surface being relatively richer in Pd. Reasons for this pattern will be presented later.

3.3.2 Energies. Fitting the calculated cluster $(PtPd)_M$ binding energies to eqn. (9), yields an a value of 5.2412 eV. This is intermediate between the E_{coh} values for bulk Pd (3.936 eV) and Pt (5.853 eV),[47] which is to be expected, since we have taken the energy scaling parameters for Pt–Pd interactions (A and ζ) as the average of those for Pt–Pt and Pd–Pd. From the experi-

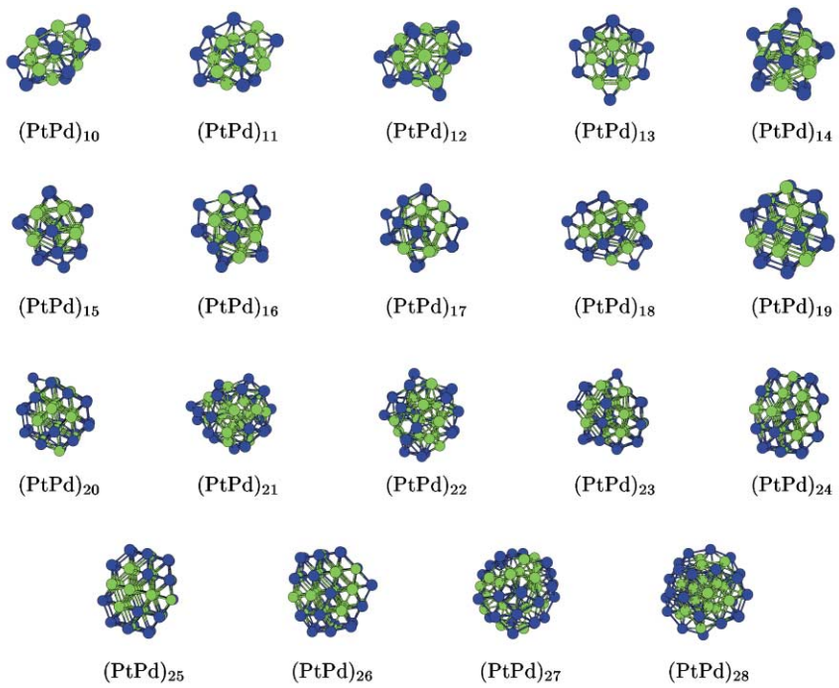

Fig. 5 GM for Pt–Pd nanoalloy clusters $(PtPd)_5$–$(PtPd)_{28}$, using Pt–Pd parameter set **I**. Colour scheme as in Figs. 1 and 3 (green = Pt; blue = Pd).

mental cohesive energies of bulk Pt and Pd and the enthalpy of formation of the bulk $Pt_{0.5}Pd_{0.5}$ phase (-4 kJ mol^{-1} [42]), we obtain an estimate for the cohesive energy of the bulk alloy phase of 4.94 eV. The a value of 5.2412 eV obtained from the fit to eqn. (9) for the $(PtPd)_M$ clusters (with only up to 56 atoms) is only 6% higher than this estimate, which is consistent with the errors previously obtained for Pt and Pd (see above). This provides some measure of support for adopting the averaged Pt–Pd Gupta parameter set (**I**) for studying Pt–Pd alloys and nanoalloy clusters.

A plot of the difference between the fit to eqn. (9) and the calculated binding energies ($E_{\rm fit} - E_b$) is shown in Fig. 6, as a

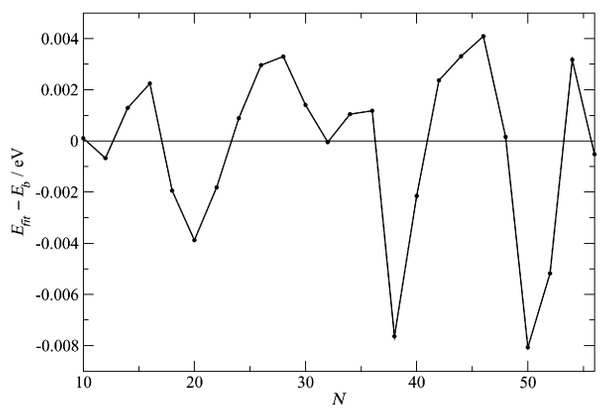

Fig. 6 Plot of $E_{\rm fit} - E_b$ as a function of N ($= 2M$) for $(PtPd)_M$ clusters, using Pt–Pd parameter set **I**.

function of the total number of atoms. The range of oscillations in this plot is significantly smaller than previously observed for Pt and Pd clusters, but there are significant troughs (indicating relative stability) for N = 20, 38 and 50. These nuclearities also show up as peaks in a plot (not shown) of the second difference in the binding energies ($\Delta_2 E_b$) against N. As discussed above, the 38- and 50-atom clusters have structures based on fcc packing and have symmetrical, closed-shell-type structures, which explains their stability. The 20-atom cluster $(PtPd)_{10}$, however, has a structure (see Fig. 5) corresponding to a Pt-centred $Pt_{10}Pd_3$ icosahedron, which is capped by seven Pd atoms. Fig. 6 also shows that there are a number of structures (centred at around 28 atoms and 44 atoms) which have lower than average stabilities (*i.e.* with $E_b < E_{\rm fit}$). The clusters with 26–36 atoms have structures based on decahedral packing, which suggests that this is not a particularly stable motif, though it appears that there is not a competitive icosahedral or fcc structure in this range. As mentioned above, $(PtPd)_{21}$ and $(PtPd)_{22}$ have fairly disordered structures based on icosahedral packing, while $(PtPd)_{23}$ has a distorted fcc-type arrangement of atoms. These structures are clearly less stable than the extrapolated 'average' structure and the symmetrical fcc isomers of $(PtPd)_{19}$ and $(PtPd)_{25}$. It is also noteworthy that the 54- and 56-atom clusters, which are based on the 2-shell Mackay icosahedron also have less than average stability, which is consistent with the fact that fewer icosahedral structures are found for $(PtPd)_M$ clusters, as compared with pure Pt and Pd clusters.

3.4 Investigation of specific non-stoichiometric Pt–Pd clusters

As shown in Fig. 5, the structure of $(PtPd)_{14}$ is based on a 19-atom (decahedral) stack of two pentagonal prisms, with two axial capping atoms and two central atoms. (This structure is related to the DI by a twist of the central pentagon.) This 19-atom core is then capped on nine of its ten square faces. The next stoichiometric cluster, $(PtPd)_{15}$, has two extra atoms, one capping the remaining square face and one bridging two of the caps. Because of the structures found for these 28- and 30-atom clusters, it was decided to search for the GM of the non-stoichiometric 29-atom clusters $Pt_{15}Pd_{14}$ and $Pt_{14}Pd_{15}$, in order to determine whether the intermediate structure has all ten square faces capped. Fig. 7 shows that the GM for both

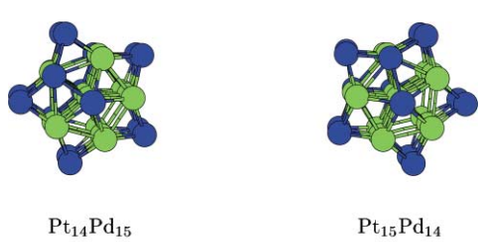

Fig. 7 Twenty-nine-atom Pt–Pd clusters with capped decahedral GM structures, using Pt–Pd parameter set **I**.

compositions has the expected structure – an omnicapped pentagonal pyramidal stack, with D_{5h} symmetry (ignoring the Pt–Pd colouring pattern). This star-shaped geometry has previously been found as the GM for 29-atom clusters modelled by a short-ranged Morse potential,[50] and for Au clusters, using the MM many-body potential,[57] though they have not previously been found in our studies using the Gupta potential for alloy or elemental clusters.[55,56,59,67] Finally, it should be noted that both compositional isomers (or 'composomers'[56]), along with the 28- and 30-atom clusters, have Pt atoms at both interstitial sites and Pd atoms on all of the more exposed sites (*i.e.* the axial positions and the square-face-capping sites).

As mentioned above, the GM found for $(PtPd)_{27}$ and the lowest metastable isomers of $(PtPd)_{28}$ are based on the 2-shell Mackay icosahedron, with one atom removed or added, respectively. It was decided to search for the GM of the non-stoichiometric 55-atom clusters $Pt_{28}Pd_{27}$ and $Pt_{27}Pd_{28}$ in order to confirm that the complete 2-shell icosahedron is the most stable structure for 55 atoms. As shown in Fig. 8, both composomers do adopt the icosahedral structure, in which the surface atoms are predominantly Pd atoms and the interior sites are mostly occupied by Pt atoms. This structure was also found to be the GM for Pd_{55}, though not for Pt_{55}. It should be noted, however, that in both cases (as in the 54- and 56-atom clusters), the atom at the very centre of the cluster is a Pd atom (see discussion below).

Fig. 8 Fifty-five-atom Pt–Pd clusters with 2-shell icosahedral GM structures, using Pt–Pd parameter set **I**.

3.5 Structural effects of varying the composition of 14-atom Pd–Pt clusters

Comparison of Figs. 1, 3 and 5 reveals that 14-atom Pt, Pd and Pt–Pd clusters have different geometries: Pt_{14} is a hexagonal antiprism, Pd_{14} is a capped icosahedron and $(PtPd)_7$ has a unique non-icosahedral structure which is based on polytetrahedral packing. It was decided that the 14-atom clusters would be a good system to study to investigate the variation in the geometric structure of the GM as a function of composition.

Fig. 9 shows the lowest energy structures obtained for clusters of composition Pt_xPd_{14-x}, for $0 \leq x \leq 14$. Starting from Pt_{14}, doping a single Pd atom into the cluster changes the structure of the GM from the haxagonal antiprism to the capped icosahedron, with the Pd atom occupying the capping site. This is consistent with previous studies on 13- and 14-atom Cu–Au clusters by López *et al.*[18] and by our calculations on 14-, 16- and 55-atom Cu–Au clusters,[55] where it was found that the replacement of a single Au atom by Cu was sufficient to change the geometry of the GM from that of the pure Au to that of the pure Cu cluster. Similar results have also been found for Ni–Al clusters.[9,59,68] Upon substituting more Pt atoms by Pd, the capped icosahedral structure is maintained as the GM, with the lowest energy homotops all having a Pd atom in the capping site and a Pt atom in the interstitial site. The capped icosahedral structure is the GM up to Pt_9Pd_5. There is a tendency for Pd atoms to avoid each other, on the surface of the cluster – which will be discussed below.

Doping Pt atoms into Pd_{14} maintains the capped icosahedron as the GM up to Pt_3Pd_{11}. The first Pt atom occupies the interstitial site and subsequent Pt atoms occupy surface positions other than the capping site, while in Pt_3Pd_{11}, the lowest energy homotop has all three Pt atoms bonded to each other, and the two surface atoms are adjacent to the capping Pd atom. These factors will also be discussed below.

For intermediate compositions (Pt_4Pd_{10}–Pt_8Pd_6), non-icosahedral structures are found (as discussed above for the case of Pt_7Pd_7), though these structures are still based on polytetrahedral packing and regions of pentagonal symmetry. Three distinct structures are observed, with Pt_7Pd_7 and Pt_8Pd_6 having the same geometry. Similar alternations of structure type with composition have been found for 17- and 18-atom Ni–Al clusters,[59] though Jellinek and colleagues have shown that the GM of 14-atom Ni–Al clusters maintain the same capped icosahedral geometry for all compositions.[68] In this intermediate range, there is also a tendency for Pd atoms to be located on the surface of the cluster, with Pt atoms in the interior.

3.6 Homotop stability: segregation *vs.* ordering in Pt–Pd clusters

In the preceding sections, a number of trends have been noted regarding the distribution of Pt and Pd atoms in Pt–Pd nanoalloy clusters. To recap, the general finding is that there is a tendency (as manifest in the lowest energy isomers found by the GA) for segregation to occur: with Pd atoms preferentially occupying surface sites and Pt atoms preferentially occupying interior sites (*i.e.* finite Pt–Pd clusters are not random solid solutions). In this section we will explain this observation along with other, more specific points mentioned above.

Previous studies of nanoalloy clusters[9,15,43,55,59,68–70] have shown that homotop stability – *i.e.* whether there is segregation or mixing (which may be ordered or random) of the unlike atoms (A and B) – is determined by a number of factors, which, depending on the geometry, size and composition of the cluster and the nature of atoms A and B, may oppose or reinforce each other.

- Maximization of the number of the strongest interatomic interactions.
- Minimization of the cluster surface energy – this favours segregation, with the cluster surface becoming richer in the element which has the lower surface energy.
- Minimization of bulk strain – this favours the location of the smaller atom at the centre of icosahedral clusters, for example.

The observed tendency for the segregation of Pd atoms to the surface, and Pt to the core of Pt–Pd clusters is driven by the first two of these factors. The surface energy of Pd (125–131 meV $Å^{-2}$) is significantly lower than that of Pt (155–159 meV $Å^{-2}$)[71–73] and having Pt atoms in the core also enables the number of Pt–Pt interactions (the strongest interactions when using Gupta Pt–Pd parameter set **I**) to be maximized. The greater strength of the Pt–Pt interactions, as compared with Pd–Pd, is manifest in the higher cohesive energy of bulk Pt.[49] The observation that (for low Pd concentrations) the Pd atoms tend to avoid each other can likewise be explained in terms of minimizing the number of weak Pd–Pd interactions, while leaving the highest number of strong Pt–Pt interactions. The avoidance of low-coordinate capping sites by Pt and the tendency for Pt atoms to aggregate maximizes the number of strong Pt–Pt interactions, while the preferred location of Pt atoms adjacent to capping Pd atoms increases their coordination and, hence, the number of (second strongest) Pt–Pd interactions.

Considering the third factor mentioned above: the inner atoms in icosahedral clusters of single elements tend to be under compression, so as to maximize surface atom interactions.[74–76] This leads to a destabilizing bulk strain energy,[75] which increases with increasing cluster size so there is generally a preference for smaller atoms to occupy these sites, thereby

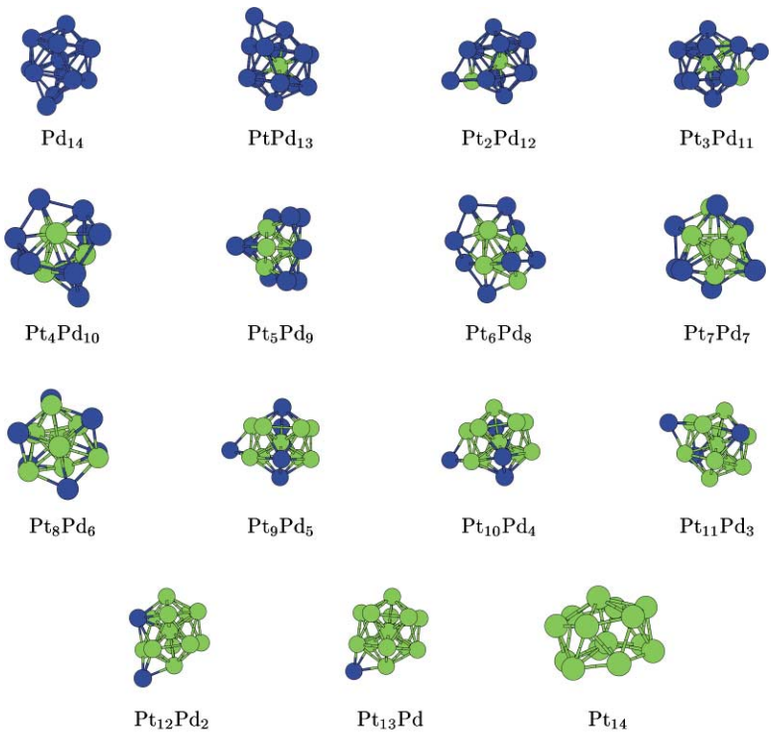

Fig. 9 GM for 14-atom Pt–Pd clusters Pt_xPd_{14-x} ($0 \leq x \leq 14$), using Pt–Pd parameter set **I**.

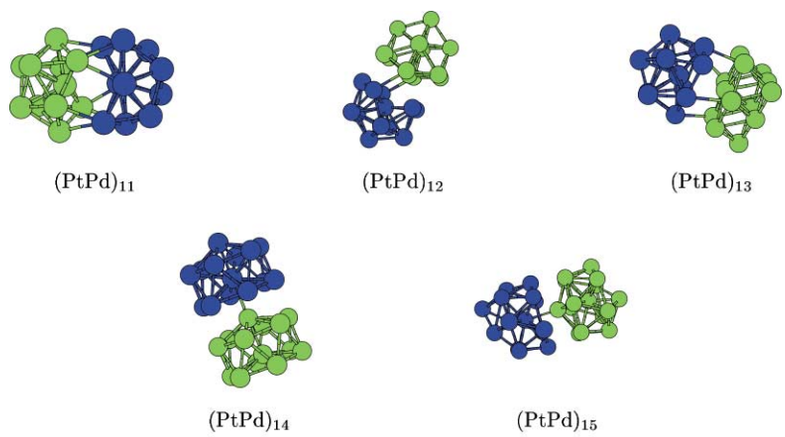

Fig. 10 GM for Pt–Pd nanoalloy clusters $(PtPd)_{11}$–$(PtPd)_{15}$, using Pt–Pd parameter set **II**.

relieving the strain.[55,59] This may explain why the (very) slightly smaller Pd atom [r(Pd) = 1.38 Å, r(Pt) = 1.39 Å [49]] occupies this site in $Pt_{27}Pd_{28}$ and $Pt_{28}Pd_{27}$, despite the general tendency for Pd atoms to lie on the surface of the cluster. It should be noted, however, that EAM studies by Rey *et al.* predict that the most stable homotop of the 2-shell icosahedral $Ni_{54}Al$ cluster is that in which the Al atom occupies the inner-most interstitial site (despite Al being larger and having a lower surface energy than Ni).[69] This was attributed to the maximization of Ni–Al interactions when the Al atom occupies a 12-coordinate site. For Pd–Pt parameter set **I**, however, the Pt–Pt interaction is stronger than Pt–Pd, so this argument would not be expected to apply.

The prediction that Pt–Pd nanoalloy clusters should exhibit shell-like segregation, with a surface shell which is rich in Pd and a core shell which is rich in Pt, is consistent with the experimental studies of Renouprez, Rousset and colleagues on Pt–Pd particles.[25,26] This segregation also explains why there are more Pt–Pt bonds than Pt–Pd or Pd–Pd bonds. The fact that, experimentally, segregation is seen to be greatest for larger clusters may be because, as suggested by Gijzeman,[77] the gain in energy on moving an atom from an internal to an external site is small in smaller clusters, where the internal sites are not truly bulk-like. Finally, it should be noted that DFT calculations by Ruban *et al.* also indicate an energetic preference for the segregation of Pt impurity atoms into the bulk, when they are doped into Pd, though no strong surface segregation was calculated for Pd impurities doped into Pt.[10] The calculated segregation tendency was found to be less in the Pt–Pd system than in Cu–Au, which is consistent with our results for Pt–Pd and Cu–Au nanoalloys.[55]

3.7 Variation of the Pt–Pd Gupta potential parameters

The results that we have obtained, and the conclusions that we have drawn, concerning the geometrical structures and atomic ordering in Pt–Pd nanoalloys, has been based solely on the use of the averaged Pt–Pd Gupta parameters (set **I**). While we believe that these parameters give a good qualitative description of Pt–Pd clusters, we have performed a limited test of the effect of changing the Pt–Pd Gupta parameters on the structures and segregation or mixing of the alloy clusters, using Gupta Pt–Pd parameter sets **II** and **III** (see Table 1).

Fig. 10 shows the lowest energy isomers obtained for $(PtPd)_M$ clusters, with M = 11–15, for parameter set **II**, in which the 2-body repulsive energy scaling parameter (A) for Pt–Pd is

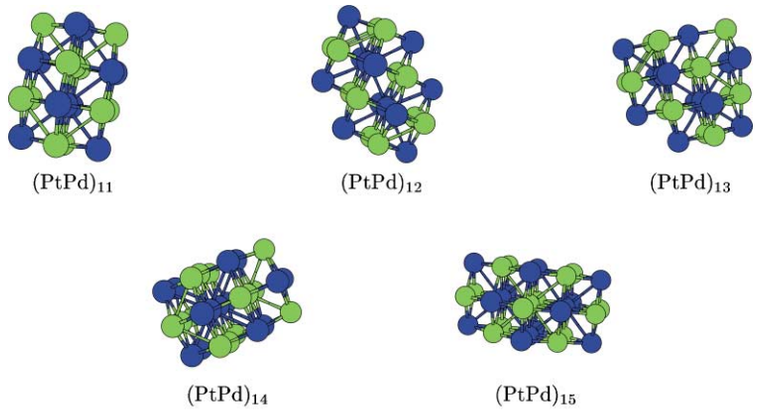

Fig. 11 GM for Pt–Pd nanoalloy clusters $(PtPd)_{11}$–$(PtPd)_{15}$, using Pt–Pd parameter set **III**.

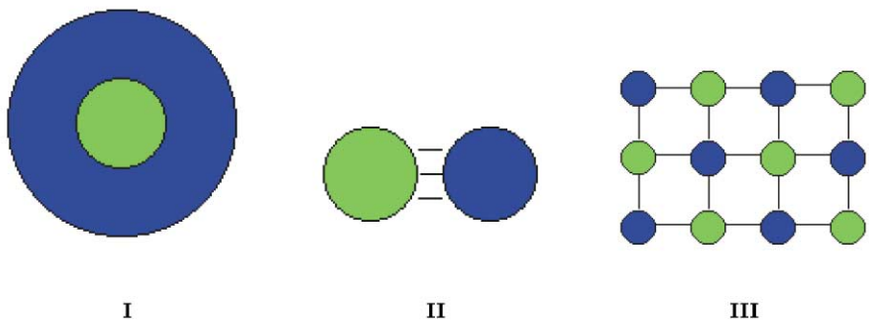

Fig. 12 Schematic representation of the idealized atomic ordering/segregation found for Pt–Pd nanoalloy clusters, using Pt–Pd parameter sets **I**, **II** and **III**. (Green shading = Pt, blue shading = Pd.)

larger than both the Pt–Pt and the Pd–Pd values. The effect of this change is to destabilize Pt–Pd interactions relative to Pt–Pt and Pd–Pd, so that the clusters are completely segregated, forming two compact Pt_M and Pd_M sub-clusters, connected by a small number of Pt–Pd bonds. This segregation is distinct from that observed for parameter set **I**, where the Pd atoms tend to segregate into a shell surrounding a Pt core. The Pt and Pd sub-clusters have very similar structures, often based on icosahedral or hexagonal antiprismatic fragments. The $(PtPd)_{14}$ cluster is of particular interest. Both the Pt and the Pd sub-clusters have the hexagonal antiprismatic structure previously observed for Pt_{14}, even though the preferred structure for Pd_{14} is the capped icosahedron. Similarly, in $(PtPd)_{13}$, both sub-clusters have this antiprismatic arrangement (with one atom missing), rather than the icosahedral structure adopted by both Pt_{13} and Pd_{13}. Presumably these alternative structures are observed because they enable stronger inter-fragment bonding.

Fig. 11 shows the lowest energy isomers obtained for $(PtPd)_M$ clusters, with M = 11–15, for parameter set **III**, in which the many-body attractive energy scaling parameter (ζ) for Pt–Pd is larger than both the Pt–Pt and the Pd–Pd values. The effect of this change is to favour mixing of the Pt and Pd atoms, so as to maximize the number of strong Pt–Pd bonds. In this case, the mixing is ordered, giving rise to novel structures with alternating arrangements of Pt and Pd atoms, although there are still relatively short Pt–Pt and Pd–Pd distances. In fact, the packing of the atoms in these clusters is body-centred cubic (bcc), with the Pt and Pd atoms lying on interpenetrating simple cubic lattices, such that each Pt atom is surrounded by a cube of Pd atoms and *vice versa*. This CsCl-type ordered arrangement of atoms, which is known as the β-brass (β-CuZn) or B2 structure in alloys,[6] has not been observed for bulk PtPd alloys.

The three general types of structures of Pt–Pd clusters, which are favoured by parameter sets **I**, **II** and **III**, are depicted schematically in Fig. 12. Parameter set **I** favours structures which can be described ideally as shell-segregated, with a shell of Pd atoms surrounding a core of Pt atoms (though there is some mixing between the shells). As discussed above, the important factors favouring these structure-types are the lower surface energy of Pd and the higher cohesive energy of Pt. Parameter set **II** favours segregated structures consisting of Pt and Pd sub-clusters with only a small number of Pt–Pd bonds. This is driven by the greater Pt–Pd pair repulsion term. Finally, parameter set **III** favours Pt–Pd mixing and an ordered arrangement of Pt and Pd atoms, due to the high many-body Pt–Pd cohesive energy. Of the three parameter sets tested here, set **I** clearly yields structures and segregation patterns which are in closest agreement with experiment.[25,26] In future, this parameter set could be refined by including cohesive and elastic properties of bulk Pt–Pd alloys in the potential fitting.

Previous theoretical studies of Cu–Au nanoalloys, using the Gupta potential, have shown that shell segregation occurs,[55] with the extent of segregation being slightly greater than that calculated here for Pt–Pd clusters. Although the Au–Au interactions are the strongest, the higher surface energy of Au compared with Cu, and the greater difference in atomic sizes, favours Cu-rich cores surrounded by Au-rich shells – *i.e.* the reverse situation to that observed for Pt–Pd clusters, where the heavier, more tightly bound element (Pt) is found in the core. The optimized Cu–Au interaction parameters (based on fitting properties of Cu_3Au[47]) are such that the pair and many-body energy scaling parameters (A = 0.1539 eV, ζ = 1.5605 eV) are close to the average of the Cu–Cu and Au–Au parameters (A_{ave} = 0.15 eV, ζ_{ave} = 1.51) – as assumed for Pt–Pd parameter set **I**. This average nature of the energy scaling parameters is consistent with the small enthalpy of formation measured experimentally for Cu_3Au (-7.2 kJ mol^{-1} [78]). In contrast to Pt–Pd parameter set **I**, however, the Cu–Au 2-body range exponent (p) is greater than that of both Cu and Au, rather than being the average,[47] so the heteronuclear repulsive interaction dies off more quickly than the homonuclear interactions. The many-body range exponent (q) for Cu–Au is intermediate between the pure element values.

In the case of Ni–Al nanoalloys, the Gupta potential again favours segregation (though this is less complete than for Pt–Pd or Cu–Au clusters). The core is generally richer in the element

(Ni) with the highest bulk cohesive energy and surface energy[9,59,68,69,79] – as in Pt–Pd clusters. As for Pt–Pd parameter set **I**, all of the Ni–Al Gupta parameters are intermediate between those of the two elements,[47] though they are not averages. The fact that the Ni–Al A value is small (0.0563 eV) and similar to that of Ni (0.0376 eV) and that the ζ value (1.2349 eV) is larger than that of Ni (1.070 eV) results in the Ni–Al interaction being stronger than the Ni–Ni and Al–Al interactions. This is consistent with the relatively high exothermic enthalpy of formation of Ni_3Al (-37.6 kJ mol^{-1} [78]) and the fact that its cohesive energy is higher than that of Ni and Al.[47] The reduced segregation is caused by the greater strength of the Ni–Al interactions, which favours mixing,[9,68,69] though not to the extent found for Pt–Pd parameter set **III**. Interestingly, the most stable structure for the bulk phase of NiAl is the ordered bcc (B2) structure – as observed for Pt–Pd clusters using parameter set **III**. Calculations on near stoichiometric (1:1) Ni–Al clusters, however, do not show any evidence for this type of structure for small clusters.[59]

It is worth noting that ordered bulk Cu–Au phases are only stable below approximately 500–600 K, whereas bulk Ni–Al alloys are ordered up to high temperatures.[78] These facts, along with the non-existence of ordered Pt–Pd phases (even at low temperatures), are consistent with the relative tendencies towards ordering which have been calculated for finite Ni–Al, Cu–Au and Pt–Pd clusters.

Turning to related alloy systems, calculations by Montejano-Carrizalez *et al.* using the EAM model, have indicated that Cu–Ni nanoalloy clusters undergo shell segregation, with the surface becoming richer in Cu and the core richer in Ni.[15] The situation for Cu–Pd clusters, however, is less clear cut. Montejano-Carrizalez *et al.* have concluded that the atomic distribution in Cu–Pd clusters, is determined by the interplay of two factors: [15] the tendency for Pd to segregate to the surface (as in Cu–Pd alloys, despite Cu having the lower surface energy [72]) and the tendency to form ordered bulk phases at low temperatures (as in the case of Cu–Au alloys).[78] CEM calculations by Zhu *et al.*, however, have led to the prediction that the surfaces of Cu–Pd nanoalloys should be Cu-rich (due to the lower surface energy of Cu), with the second layer being Pd-rich, so as to maximize Cu–Pd mixing.[80] These later calculations appear to be in better agreement with experiment: TEM and EXAFS studies by Molenbroek *et al.* show that on alumina supports Cu–Pd particles have Cu-rich surfaces, while on alumina supports the particles are better described as random alloys.[12]

4 Conclusions

From our global optimization studies, using a Genetic Algorithm and describing interatomic interactions by the Gupta many-body potential, pure clusters of platinum and palladium have been predicted to adopt a variety of structures, depending on the cluster size. Many of the structures are regular (ordered), though there is a tendency (which is greater for Pt than for Pd) towards forming disordered structures. The relative propensity of Pt and Pd clusters to adopt disordered (amorphous) structures has been discussed and comparisons made with previous studies of Cu and Au clusters. Another difference between the two metals is the increased tendency for Pd to form clusters based on icosahedral packing. Our calculated lowest energy structures for the pure metal clusters have been shown to be in good qualitative agreement with previous theoretical calculations and experimental studies on Pt and Pd clusters.

Obtaining a set of Gupta potential parameters for Pt–Pd interactions by averaging those for Pt–Pt and Pd–Pd interactions, we find that the predicted lowest energy structures for $(PtPd)_M$ nanoalloy clusters generally have different geometric structures than the corresponding pure Pt or Pd clusters: with a reduced tendency to display icosahedral packing and a larger number of capped decahedral structures. Compared with Pd, there is also an increase in the number of disordered structures for the Pt–Pd clusters. Shell-like atomic segregation is favoured for these Pt–Pd clusters, with the surface becoming richer in Pd and the core becoming richer in Pt. This segregation, which is consistent with experimental studies on Pt–Pd particles, has been explained in terms of the lower surface energy of Pd and the greater cohesive energy of Pt. For non-stoichiometric Pt–Pd clusters, the calculated global minimum has been shown to depend strongly on the composition, with the doping of even a single Pt atom into a Pd cluster (or *vice versa*) being sufficient to change the geometrical structure of the cluster.

Finally, it has been shown that varying the Pt–Pd interaction parameters of the Gupta potential can have very significant effects on the geometrical structures (including the degree of geometrical order or disorder) and the tendency towards ordering or segregation (of the Pt and Pd atoms) of Pt–Pd clusters. These findings have been compared with previous theoretical results for a number of binary nanoalloy systems. The first Pt–Pd parameter set used (obtained by averaging the Pt–Pt and Pd–Pd parameters) yields geometrical structures and Pt–Pd segregation which agree well with experimental microscopy and EXAFS measurements. In future, this parameter set could be refined by including cohesive and elastic properties of bulk Pt–Pd alloys in the potential fitting.

Acknowledgements

T. V. M.-J. is grateful to The School of Chemical Sciences, University of Birmingham, for a School Studentship, and to Hewlett-Packard Co. (Galway, Ireland) for sponsorship. The authors wish to thank Dr Christopher Roberts for development of the GA code and Graham Cox for help in preparing some of the figures.

References

1 R. L. Johnston, *Atomic and Molecular Clusters*, Taylor and Francis, London, 2002.
2 B. V. Reddy, S. N. Khanna and B. I. Dunlap, *Phys. Rev. Lett.*, 1993, **70**, 3323.
3 M. Moseler, H. Häkkinen, R. N. Barnett and U. Landman, *Phys. Rev. Lett.*, 2001, **86**, 2545.
4 J. Jortner, *Z. Phys. D*, 1992, **24**, 247.
5 R. L. Johnston, *PhilosTrans. R. Soc. London, Ser. A*, 1998, **356**, 1998.
6 W. B. Pearson, *The Crystal Chemistry and Physics of Metals and Alloys*, Wiley, New York, 1972.
7 S. Giorgio, H. Graoui, C. Chapan and C. R. Henry, in *Metal Clusters in Chemistry*, P. Braunstein, L. A. Oro and P. R. Raithby, ed., Wiley-VCH, Weinheim, 1999, vol. 2, p. 1194.
8 B. Pauwels, G. Van Tendeloo, E. Zhurkin, M. Hou, G. Verschoren, L. Theil Kuhn, W. Bouwen and P. Lievens, *Phys. Rev. B*, 2001, **63**, 165406.
9 J. Jellinek and E. B. Krissinel, in *Theory of Atomic and Molecular Clusters*, J. Jellinek, ed., Springer, Berlin, 1999, p. 277.
10 A. V. Ruban, H. L. Skriver and J. K. Nørskov, *Phys. Rev. B*, 1999, **59**, 15990.
11 G. Bozzolo, J. Ferrante, R. D. Noebe, B. Good, F. S. Honecy and P. Abel, *Comput. Mater. Sci.*, 1999, **15**, 169.
12 A. M. Molenbroek, S. Haukka and B. S. Clausen, *J. Phys. Chem. B*, 1998, **102**, 10680.
13 G. Schmid, in *Metal Clusters in Chemistry*, P. Braunstein, L. A. Oro and P. R. Raithby, ed., Wiley-VCH, Weinheim, 1999, vol. 3, p. 1325.
14 M. P. Andrews and S. C. O'Brien, *J. Phys. Chem.*, 1992, **96**, 8233.
15 J. M. Montejano-Carrizalez, M. P. Iñiguez and J. A. Alonso, *Phys. Rev. B*, 1994, **49**, 16649.
16 L. Zhu and A. E. DePristo, *J. Chem. Phys.*, 1995, **102**, 5342.
17 A. Christensen, P. Stolze and J. K. Nørskov, *J. Phys. Condens. Matter*, 1995, **7**, 1047.
18 M. J. López, P. A. Marcos and J. A. Alonso, *J. Chem. Phys.*, 1996, **104**, 1056.
19 E. B. Krissinel and J. Jellinek, *Int. J. Quantum Chem.*, 1997, **62**, 185.
20 A. Fortunelli and A. M. Velasco, *J. Mol. Struct. (THEOCHEM)*, 1999, **487**, 251.

21 M. Calleja, C. Rey, M. M. G. Alemany, L. J. Gallego, P. Ordejón, D. Sánchez-Portal, E. Artacho and J. M. Soler, *Phys. Rev. B*, 1999, **60**, 2020.
22 S. Bromley, G. Sankar, C. R. A. Catlow, T. Maschmeyer, B. F. G. Johnson and J. M. Thomas, *Chem. Phys. Lett*, 2001, **340**, 524.
23 B. Coq and F. Figueras, *J. Mol. Catal. A*, 2001, **173**, 117.
24 A. Stanislaus and B. H. Cooper, *Catal. Rev. Sci. Eng.*, 1994, **36**, 75.
25 A. J. Renouprez, J. L. Rousset, A. M. Cadrot, Y. Soldo and L. Stievano, *J. Alloys Compd.*, 2001, **328**, 50.
26 J. L. Rousset, L. Stievano, F. J. Cadete Santos Aires, C. Geantet, A. J. Renouprez and M. Pellarin, *J. Catal.*, 2001, **202**, 163.
27 A. Sachdev, R. I. Masel and J. B. Adams, *Z. Phys. D*, 1993, **26**, 310.
28 J. P. K. Doye and D. J. Wales, *New J. Chem.*, 1998, 733.
29 S. H. Yang, D. A. Drabold, J. B. Adams, P. Ordejón and K. Glassford, *J. Phys.: Condens. Matter*, 1997, **9**, L39.
30 J. Kua and W. A. Goddard, *J. Phys. Chem. B*, 1998, **102**, 9481.
31 X. Lin, N. J. Ramer, A. M. Rappe, K. C. Hass, W. F. Schneider and B. L. Trout, *J. Phys. Chem. B*, 2001, **105**, 7739.
32 J. García-Rodeja, C. Rey, L. J. Gallego and J. A. Alonso, *Phys. Rev. B*, 1994, **49**, 8495.
33 J. Uppenbrink and D. J. Wales, *Z. Phys. D*, 1993, **26**, 258.
34 L. Q. Yang and A. E. DePristo, *J. Chem. Phys.*, 1994, **100**, 725.
35 N. Watari and S. Ohnishi, *Phys. Rev. B*, 1998, **58**, 1665.
36 H. Graoui, S. Giorgio and C. R. Henry, *Surf. Sci.*, 1998, **417**, 350.
37 W. Contrata, M. J. Mitchell and J. M. Mochel, *Ultramicroscopy*, 1993, **48**, 297.
38 M. S. Stave and A. E. DePristo, *J. Chem. Phys.*, 1992, **97**, 3386.
39 I. Efremenko, *J. Mol. Catal. A*, 2001, **173**, 19.
40 J. M. Penisson and A. Renou, *J. Cryst. Growth*, 1990, **102**, 585.
41 M. José-Yacamán, M. Marín-Almazo and J. A. Ascencio, *J. Mol. Catal. A*, 2001, **173**, 61.
42 F. R. de Boer, R. Boom, W. C. M. Mattens, A. R. Miedeama and A. K. Niessen, *Cohesion in Metals: Transition Metal Alloys*, Elsevier, Amsterdam, 1988.
43 N. T. Wilson and R. L. Johnston, *J. Mater. Chem.*, 2002, **12**, 2913.
44 B. Hartke, *Chem. Phys. Lett.*, 1996, **258**, 144.
45 J. Holland, *Adaptation in Natural and Artificial Systems*, University of Michigan Press, Ann Arbor, MI, 1975.
46 D. E. Goldberg, *Genetic Algorithms in Search, Optimization and Machine Learning*, Addison-Wesley, Reading, MA, 1989.
47 F. Cleri and V. Rosato, *Phys. Rev. B*, 1993, **48**, 22.
48 R. L. Johnston and C. Roberts, in *Soft Computing Approaches in Chemistry*, H. Cartwright and L. Sztandera, ed., Physica-Verlag, Heidelberg, in press.
49 C. Kittel, *Introduction to Solid State Physics*, John Wiley, New York, 6th edn., 1986.
50 C. Roberts, R. L. Johnston and N. T. Wilson, *Theor. Chem. Acc.*, 2000, **104**, 123.
51 R. H. Byrd, P. Lu, J. Nocedal and C. Zhu, *SIAM J. Sci. Comput.*, 1995, **16**, 1190.
52 J. P. K. Doye and D. J. Wales, *J. Phys. Chem. A.*, 1997, **101**, 5111.
53 Z. Li and H. A. Scheraga, *J. Mol. Struct. (THEOCHEM)*, 1998, **179**, 333.
54 D. M. Deaven and K. M. Ho, *Phys. Rev. Lett.*, 1995, **75**, 288.
55 S. Darby, T. V. Mortimer-Jones, R. L. Johnston and C. Roberts, *J. Chem. Phys.*, 2002, **116**, 1536.
56 R. A. Lordeiro, F. F. Guimarães, J. C. Belchior and R. L. Johnston, manuscript in preparation.
57 N. T. Wilson and R. L. Johnston, *Eur. Phys. J. D*, 2000, **12**, 161.
58 L. D. Lloyd and R. L. Johnston, *J. Chem. Soc., Dalton Trans.*, 2000, 307.
59 M. S. Bailey, N. T. Wilson, C. Roberts and R. L. Johnston, *Eur. Phys. J. D*, submitted.
60 S. Abbet, A. Sanchez, U. Heiz and W.-D. Schneider, *J. Catal.*, 2001, **198**, 122.
61 K. Michaelian, N. Rendón and I. L. Garzón, *Phys. Rev. B*, 1999, **60**, 2000.
62 I. L. Garzón, K. Michaelian, M. R. Beltrán, A. Posada-Amarillas, P. Ordejon, E. Artacho, D. Sanchez-Portal and J. M. Soler, *Phys. Rev. Lett.*, 1998, **81**, 1600.
63 D. Zanchet, B. D. Hall and D. Ugarte, *J. Phys. Chem. B*, 2000, **104**, 11013.
64 J. M. Soler, M. R. Beltrán, K. Michaelian, I. L. Garzón, P. Ordejón, D. Sánchez-Portal and E. Artacho, *Phys. Rev. B*, 2000, **61**, 5771.
65 K. Michaelian, M. R. Beltrán and I. L. Garzón, *Phys. Rev. B*, 2002, **65**, 041403.
66 I. L. Garzón, K. Michaelian, M. R. Beltrán, A. Posada-Amarillas, P. Ordejon, E. Artacho, D. Sanchez-Portal and J. M. Soler, *Eur. Phys. J. D*, 1999, **9**, 211.
67 A. Posada Amarillas, M. F. Ortíz, C. Roberts, T. V. Mortimer-Jones and R. L. Johnston, manuscript in preparation.
68 E. F. Rexer, J. Jellinek, E. B. Krissinel, E. K. Parks and S. J. Riley, *J. Chem. Phys.*, 2002, **117**, 82.
69 C. Rey, J. Garca-Rodeja and L. J. Gallego, *Phys. Rev. B*, 1996, **54**, 2942.
70 A. M. Schoeb, T. J. Raeker, L. Q. Yang, X. Wu, T. S. King and A. E. DePristo, *Surf. Sci.*, 1992, **278**, L125.
71 W. R. Tyson and W. A. Miller, *Surf. Sci.*, 1997, **62**, 267.
72 A. R. Miedema, *Z. Metallkd.*, 1978, **69**, 287.
73 H. Cox, *Surf. Sci.*, 1998, **397**, 374.
74 J. Xie, J. A. Northby, D. L. Freeman and J. D. Doll, *J. Chem. Phys.*, 1989, **91**, 612.
75 J. P. K. Doye and D. J. Wales, *J. Phys. B*, 1996, **29**, 4859.
76 J. E. Hearn and R. L. Johnston, *J. Chem. Phys.*, 1997, **107**, 4674.
77 O. L. J. Gijzeman, *J. Catal.*, 1985, **92**, 409.
78 R. R. Hultgren, P. D. Desai, D. T. Hawkins, M. Gleiser and K. K. Kelley, *Selected Values of the Thermodynamic Properties of Binary Alloys*, American Society of Metals, Ohio, 1973.
79 M. S. Bailey, N. T. Wilson and R. L. Johnston, manuscript in preparation.
80 L. Zhu, K. S. Liang, B. Zhang, J. S. Bradley and A. E. DePristo, *J. Catal.*, 1997, **167**, 412.